

## EXHUMATION OF THE SCHIST OF SIERRA DE SALINAS

**MOLLY KOVER**, Smith College  
**Research Advisor:** Jack Loveless

### INTRODUCTION

Continental arcs are common tectonic elements of continental convergent margins. While these arcs are quite common, it is somewhat rare to find them in a condition that is worth sampling, which has made study of their exhumation processes difficult.

The Salinian Block is a continental arc that is almost completely intact located on the west coast of the United States in central California. Located at the central part of the block, the Sierra de Salinas and Gabilan Range are underlain by the schist of Sierra de Salinas and mesozoic granitic rocks (Barth, 2003). The block is bounded by three fault systems: to the east by the San Andreas fault, to the south by the Big Pine fault, and to the west by the Nacimiento fault (*Figure in Alan Chapman's introduction*). The block is composed of granitic and metasedimentary basement rocks. The schist originates from oceanic trench assemblages that were subducted under the continent. It is thought that the schists are "linked with the Pelona, Orocoxia, and Rand Schists of Southern California, which represent ... an accretionary wedge," [Kidder, Ducea].

The completeness of the Salinian Block makes it a good site to study emplacement mechanisms of trench sediments beneath continental arcs. It is strongly believed that the schist was underplated beneath the Salinian arc during an episode of subduction related to the Laramide Orogeny. What is less clear is how this schist came to the surface, whether it was due to fault systems, or tectonic extrusion. Through analysis of quartz fabric, microstructure, and crystallographic preferred orientation (CPO) diagrams, the exhumation history of the schist of Sierra de Salinas was traced.

### METHODS

#### Field

The schist of Sierra de Salinas is rich in quartz, biotite, and feldspars. While the schist has been located as far south as San Ardo and as far east as within a few kilometers of the San Andreas fault (Barth, 2003), most of that area is private farmland, which makes access to the outcrops quite difficult.

In summer 2016, we collected five samples from the schist of Sierra de Salinas: three from the northernmost edge, one closer to the western edge, and one closer to the eastern edge of the unit. All outcrops were weathered, so much so that some crumbled in the hand.

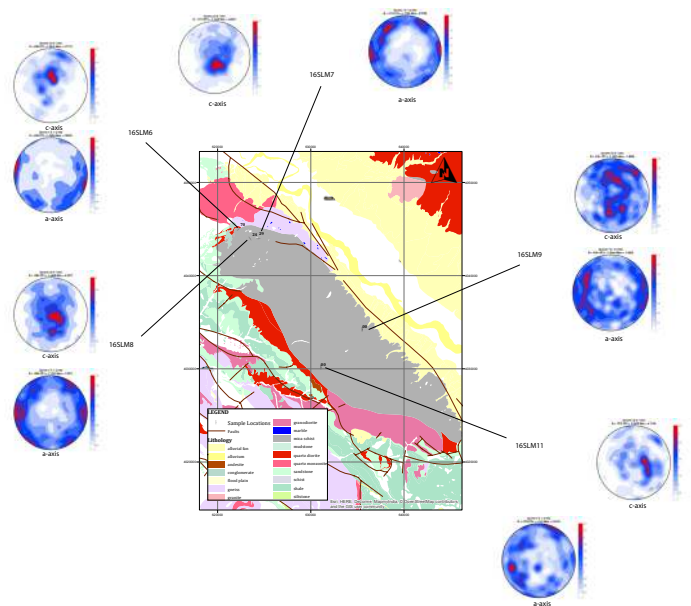


*Figure 1. Geologic Map of Schist de Sierra de Salinas generated in arcGIS. The Schist Unit appears in grey. The Sample locations are labeled with strike and dip and are attached to corresponding c- and a-axis CPO images created by MTEX*

Initially we intended to collect samples from a multiple locations within the schist unit. We followed a GPS map overlaid with a geologic map, but hit mostly dead ends along the way. Since the outcrops were few and far between, there was not much opportunity to find less weathered samples. The limited access also made the variety of location of samples practically impossible. We were limited to five outcrop locations, and therefore ended up with five samples.

### Electron Backscatter Diffraction (EBSD)

The samples were scanned using a JEOL JSM-6500F field emission Scanning Electron Microscope (SEM) and an Oxford EBSD camera in the University of Minnesota's Characterization Facility. The data was analysed with HKL Channel 5 software. The operating conditions were that of 20kV accelerating voltage, a 20 nA probe current, and a working distance of between 25 and 30 mm. Due to the deteriorated condition of the schist samples, only coarse maps were generated. The step size used for these maps was about 50 microns. The EBSD data was read in MTEX software, using a workflow written by Sarah Brownlee to generate Crystallographic Preferred Orientation (CPO) figures, or pole figures.

## RESULTS

### Description of Samples

The five samples represent three different original depths of the schist unit. Samples 6, 7, and 8, all from Dorrance Ranch (16SLM6, 16SLM7, and 16SLM8), were located near the structural top of the schist body, <1 km below the schist-bounding Salinas shear zone (Kidder and Ducea, 2006). Sample 9 (16SLM9) was collected from the deepest part of the schist unit. Together with 16SLM9, sample 11(16SLM11) is part of a two point transect that cuts horizontally across the present day surface of the unit, and from top (SLM11) to bottom (SLM9) of the structural depth.

Data was collected from the EBSD regarding the crystallographic orientation of quartz, biotite, and feldspars, but the biotite produced sparse data, and the feldspar was not consistent. Therefore, we are left to make conclusions from the quartz data alone.

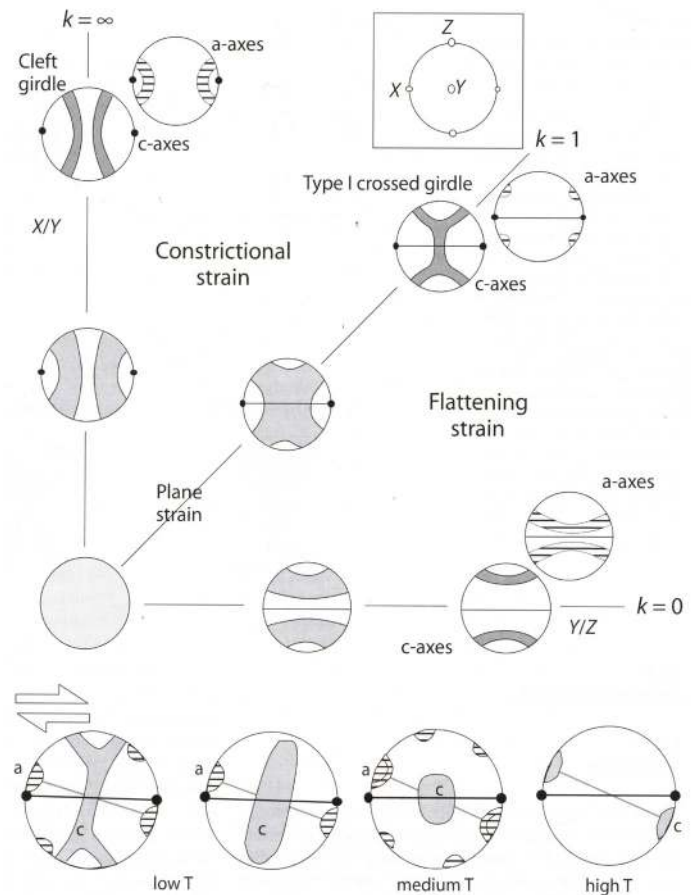


Figure 2. Flinn Diagram courtesy of Passchier and Trouw p.106.

### Sample 6

Collected from the northern part of the unit, sample 6 is a well sorted sample that is mainly fine grained. While there appears to be some ductile deformation, the sample is dominated by brittle deformation. The intracrystalline deformation of the quartz crystals indicates that they underwent some strain, the biotite some brittle fracturing, while the feldspars seem to remain mostly unchanged. There is not a clear preferred orientation along the c-axis, though a slight cross-girdle seems to be forming; the symmetrical concentrations of a-axis orientation starts to indicate a more constrictional texture (Figure 3). The more ductile deformation of the quartz in comparison to the biotite indicates that the temperature during emplacement was between the plasticity region of quartz and that of biotite.

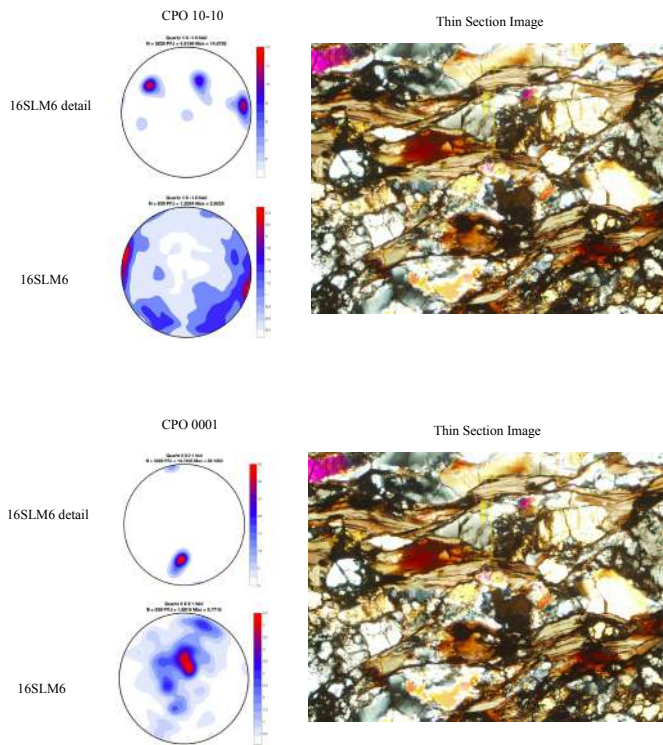


Figure 3 and 3b. Sample 6 detail and sample 6 pole figures of a-axis, c-axis, and thin section image.

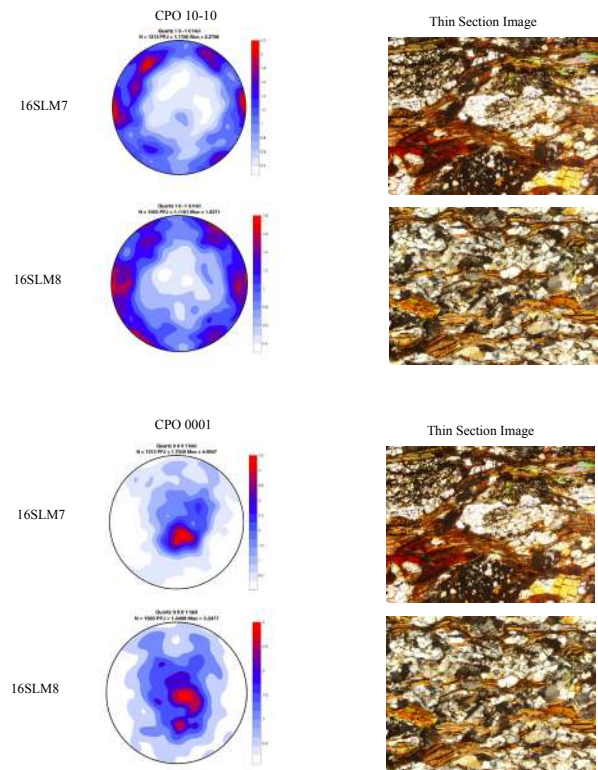


Figure 4 and 4b. Sample 7 and sample 8 pole figures of a-axis, c-axis, and thin section images

## Sample 7

Sample 7 was collected from slightly deeper in the schist, compared to sample 6. It is also well sorted but has a wider range of grain sizes, ranging from very fine to coarse. The almost fish-like shape of the biotite indicates a fair degree of ductile deformation. There is a clear preferred orientation of quartz crystals according to the c-axis diagram, but it does not line up with any of the expected distributions according to the Flinn Diagram (Figure 2). If the concentrations in the a-axis diagram were connected, it would also indicate constrictional deformation.

## Sample 8

While the grain size of sample 8 is similar to the finer grains in SLM7, and biotite, quartz, and feldspar occur in percentages similar to those of SLM7, the biotite and quartz/feldspars do not form clean bands. Instead

there are distinct bands that incorporate the biotite, quartz, and feldspars. The fractures of the biotite indicate quite brittle deformation. The c-axis pole figure for quartz displays a symmetrical cross girdle, indicative of plane strain, and the a-axis pole figure is similar to that expected from a sample undergoing plane strain.

## Sample 9

Another fine-grained sample, sample 9 is one of the least weathered samples that we collected. It held together beautifully during travel, and cutting down into a thin section. There is clear evidence of grain boundary recrystallization of the quartz crystals. The c-axis pole figures produced a symmetrical cross-girdle (Figure 5b), clear evidence of constriction. The a-axis diagram (Figure 5) had a particularly nice agreement with the Flinn Diagram (Figure 2) for constriction.

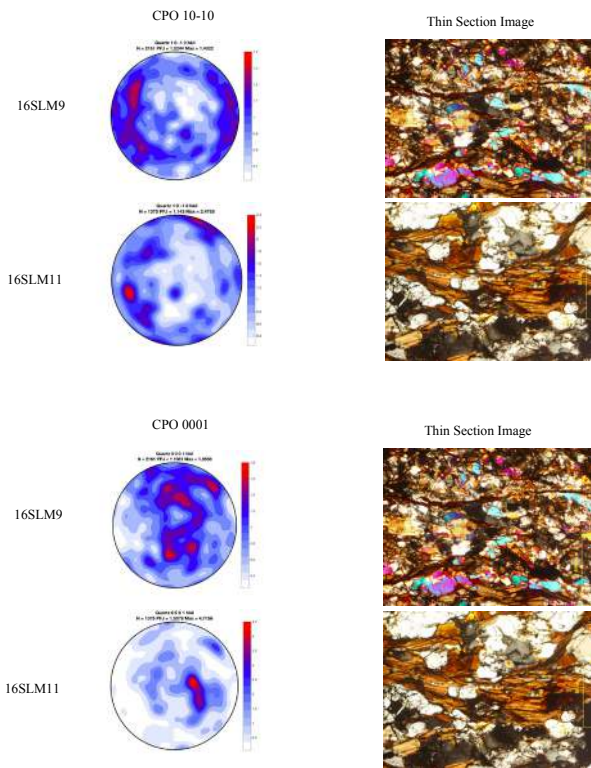


Figure 5 and 5b : Sample 9 and sample 11 pole figures of *a*-axis, *c*-axis, and thin section images.

## Sample 11

Sample 11 was the most weathered sample out of the five, requiring that we epofix it to ensure that it would hold together while we were cutting the thin section billet. The results produced are similar to the state of the sample, quite poor. The bands of biotite and quartz/feldspars are more distinct than those in SLM8, but still are not pure bands of a singular mineral, such as would be present under ductile deformation. There is a lot more feldspar in SLM11 than quartz, which also contributed to the poor CPO images generated, since we were only scanning for quartz. The pole figures generated are similar to those of the other samples — a weak, symmetrical cross-girdle — indicating somewhere between plane strain and constriction.

## DISCUSSION

### Regional Trends

The collected samples in order of relative structural depth, from top to bottom, are SLM6, SLM11, SLM8, SLM7, and SLM9. Our findings agreed with those of

Kidder and Ducea, that metamorphic grade decreases with structural depth. An inverted metamorphic field gradient was found, with SLM6 and SLM11 displaying the most ductile deformation, and SLM9 the most brittle deformation.

It was previously believed that the unit was part of the Pelona-Orocopia-Rand schists of the Mojave desert (Barth et al.), which would have involved emplacement and movement to the present day location. The well-developed quartz CPOs, the strong preferred orientation of the biotite, and the distance from their origin are indicative of strain. The clustering of the *c*-axis CPOs indicate that the shear took place at a high grade, amphibolite facies, metamorphism.

I propose that the Schist of Sierra de Salinas was that the schist was slowly underplated in stages. This would have allowed some cooling to occur, leaving the biotite to brittly deform, while it was still hot enough for the quartz to recrystallize.

## CONCLUSIONS

Barth (2003) proposed that the schist of Sierra de Salinas originated as a klippe from the basement rocks of the Mojave Desert, and that deformation occurred during Laramide tectonism. Whereas Hall (1991) insists that the deformation was more greatly influenced by oblique subduction. Further research would need to be done, particularly with a wider range of samples, and more EBSD data in order to certainly confirm one theory over the other.

## ACKNOWLEDGEMENTS

I would like to thank the Keck Consortium, Alan Chapman, and Sarah Brownlee for this opportunity. Without funding from ExxonMobil, the Keck Geology Consortium, the National Science Foundation, and Macalester College this project would not have been possible. I am infinitely grateful to my advisor Jack Loveless for his support through this project and for always pushing me to be better.

## REFERENCES

- Barth, Ander P., Joseph L. Wooden, Marty Grove, Carl E. Jacobson, and Jane N. Pedrick. "U-Pb Zircon Geochronology of Rocks in the Salinas Valley Region of California: A Reevaluation of the Crustal Structure and Origin of the Salinian Block." *Geological Society of America* 31.6 (2003): 517-20. Print.
- Hall, Clarence A., Jr. "Geology of the Point Sur-Lopez Point Region, Coast Ranges, California: A Part of the Southern California Allochthon." *Geological Society of America* (1991): n. pag. Print.
- Kidder, Steve, and Mihai Ducea. *Ongoing Work in Salinia. Ongoing Work in Salinia*. University of Arizona, n.d. Web. 12 Aug. 2016.
- Kidder, S., and Ducea, M.N., 2006, High temperatures and inverted metamorphism in the schist of Sierra de Salinas, California: *Earth and Planetary Science Letters*, v. 241, p. 422–437. doi:10.1016/j.epsl.2005.11.037
- Law, R. D., M. P. Searle, and R. L. Simpson. "Strain, Deformation Temperatures and Vorticity of Flow at the Top of the Greater Himalayan Slab, Everest Massif, Tibet." *Journal of the Geological Society, London* 161 (2004): 305-20. Print.
- Okudaira, T., T. Takeshita, and M. Toriumi. "Prism- and Basal-plane Parallel Subgrain Boundaries in Quartz: A Microstructural Geothermobarometer." *Journal of Metamorphic Geology* 16 (1998): 141-46. Print.
- Schmid, S. M., and M. Casey. "Complete Fabric Analysis of Some Commonly Observed Quartz C-axis Patterns." *Mineral and Rock Deformation: Laboratory Studies* 36 (1986): 263-86. Print.
- Passchier, C.W., Trouw, R.A., 2005. *Microtectonics*. Springer.